Free Radical Biology and Medicine 193 (2022) 23–33

Contents lists available at ScienceDirect

Free Radical Biology and Medicine

journal homepage: www.elsevier.com/locate/freeradbiomed

Proteomic analysis of skeletal muscle in Chinese hamsters with type 2 diabetes mellitus reveals that OPLAH downregulation affects insulin resistance and impaired glucose uptake

Zeya Shi [a], Yitong Huo [a], Jianan Hou [a], Ruihu Zhang [a], Jianqin Wu [a], Wentao Wang [b], Jingjing Yu [c], Hailong Wang [d], Yu Liu [e], Guohua Song [a,**], Zhenwen Chen [f,***], Zhaoyang Chen [a,*]

[a] Laboratory Animal Center, Shanxi Key Laboratory of Experimental Animal Science and Animal Model of Human Disease, Shanxi Medical University, Taiyuan, 030001, China
[b] Department of Cardiology, The Affiliated Cardiovascular Disease Hospital of Shanxi Medical University, Taiyuan, 030001, China
[c] Experimental Animal Platform in Academy of Medical Sciences, Zhengzhou University, Zhengzhou, 450052, China
[d] School of Basic Medicine, Basic Medical Science Center, Shanxi Medical University, Jinzhong, 030600, China
[e] Department of Pharmacology, Shanxi Medical University, Taiyuan, 030001, China
[f] Beijing Key Laboratory of Cancer Invasion and Metastasis Research, School of Basic Medical Science, Capital Medical University, Beijing, 100629, China

ARTICLE INFO

Keywords:
Type 2 diabetes mellitus
Chinese hamster
Skeletal muscle
Proteomics
OPLAH

ABSTRACT

Type 2 diabetes mellitus (T2DM) is a metabolic disease controlled by a combination of genetic and environmental factors. The Chinese hamster, as a novel animal model of spontaneous T2DM with high phenotypic similarity to human disease, is of great value in identifying potential therapeutic targets for T2DM. Here, we used tandem mass tag (TMT) quantitative proteomics based on liquid chromatography-tandem mass spectrometry to assess the skeletal muscles of a Chinese hamster diabetes model. We identified 38 differentially abundant proteins, of which 14 were upregulated and 24 were downregulated. Further analysis of the differentially abundant proteins revealed that five of them (OPLAH, GST, EPHX1, SIRT5, ALDH1L1) were associated with oxidative stress; these were validated at the protein and mRNA levels, and the results were consistent with the proteomic analysis results. In addition, we evaluated the role of OPLAH in the pathogenesis of T2DM in human skeletal muscle cells (HSKMCs) by silencing it. The knockdown of OPLAH caused an increase in reactive oxygen species content, decreased the GSH content, inhibited the PI3K/Akt/GLUT4 signaling pathway, and reduced glucose uptake. We propose that OPLAH downregulation plays a role in insulin resistance and glucose uptake disorders in HSKMCs possibly via oxidative stress, making it a new therapeutic target for T2DM.

1. Introduction

As the one of the most important chronic, non-communicable diseases in the world, diabetes mellitus and its complications have caused heavy economic and psychological burdens for humans [1]. According to the International Diabetes Federation, approximately 536 million people have been diagnosed with diabetes as of 2021, and this number is expected to increase to 783 million by 2045 [2]. The overwhelming majority of people with diabetes have type 2 diabetes mellitus (T2DM) [2]. T2DM is a metabolic disease caused by multiple genetic and environmental factors, for which genetic factors play an important role, mainly manifested as insulin resistance (IR) and impaired glucose uptake [3]. IR is a state in which the insulin effect in the body is lower than the normal physiological effect and mainly manifested as a decrease in the sensitivity of peripheral tissues, such as the liver, muscle, and adipose, to insulin, and decrease the ability to utilize glucose, resulting in glucose metabolism disorders [4]. Skeletal muscle tissue is the largest insulin-sensitive tissue, participates in 80% of insulin-mediated glucose uptake, and plays a critical role in maintaining systemic glucose homeostasis [5]. Thus, skeletal muscle IR plays a key role in the pathogenesis of T2DM. Researchers have conducted many studies on skeletal muscle IR and found that genes such as *Nur77*, *NOR1*, and *MG53* affect the development of T2DM through skeletal muscle IR and that drugs

* Corresponding author.
** Corresponding author.
*** Corresponding author.
E-mail addresses: ykdsgh@163.com (G. Song), czwen@ccmu.edu.cn (Z. Chen), ccytycn@163.com (Z. Chen).

https://doi.org/10.1016/j.freeradbiomed.2022.09.029
Received 30 June 2022; Received in revised form 14 September 2022; Accepted 27 September 2022
Available online 3 October 2022

Abbreviations

2-NBDG	2-[N-(7-nitrobenz-2-oxa-1,3-diaxol-4-yl) amino]-2-deoxyglucose
Akt	protein kinase B
BP	biological process
CC	cellular component
DCFH-DA	dichloro-dihydro-fluorescein diacetate
FBG	fasting blood glucose
HE	hematoxylin and eosin
HSKMC cells	human skeletal muscle cells
GLUT4	glucose transporter 4
GSH	glutathione
IR	insulin resistance
MF	molecular function
OPLAH	5-oxoprolinase
PI3K	phosphatidylinositol 3-kinase
ROS	reactive oxygen species
T2DM	type 2 diabetes mellitus
TMT	tandem mass tag

such as Yunpi Heluo decoction and exercise improve T2DM by reducing skeletal muscle IR [6–9]. However, the specific pathogenesis of IR in skeletal muscle remains unclear. Therefore, elucidating the mechanisms of skeletal muscle IR is integral for the treatment of T2DM.

From the perspectives of economics and human ethics, the establishment of animal models is indispensable for disease research, and the continuous establishment of new animal models for different diseases can advance disease research [10]. The existing commonly used animal models of T2DM, such as ob/ob and db/db mice with a single gene mutation can well simulate some characteristics of diabetes well and are very good for studying the prevention and treatment of diabetes and its complications. However, the etiology and the polygenicity of human T2DM are quite different, and thus, there are certain deficiencies and defects in the study of its etiology [11]. The inbred Chinese hamster was first reported by Meier and Yerganign in 1961, who showed that inbreeding in this group could spontaneously result in the development of diabetes, representing a new animal model of spontaneous T2DM [12]. This model conforms to the polygenic inheritance of T2DM, is characterized by non-obesity and moderately to mildly elevated blood glucose and IR, and has a similar pathogenesis and metabolic profile compared to human T2DM [13]. Previously, metabolomics and proteomics studies found that serum amino acid metabolism abnormalities and liver arachidonic acid and bile acid metabolism abnormalities in this model were consistent with human metabolic abnormalities [14,15]. Therefore, this model will bring new hope as a new T2DM animal model to find new T2DM biomarkers. Proteomics research is helpful to clarify protein changes under physiological and pathological conditions and to screen true driver genes and potential drug targets, and these have been widely applied to research on the pathogenesis of diseases [16].

In our study, to search for more potential biomarkers of T2DM, we used proteomics to detect the differentially abundant proteins in the skeletal muscle tissue of Chinese hamsters in diabetes and control groups and analyzed the differentially abundant proteins. Bioinformatics analysis showed that the identified differentially abundant proteins were significantly enriched in metabolic pathways, including purine metabolism, glutathione metabolism, and the metabolism of xenobiotics by cytochrome P450 pathways, of which glutathione metabolism and the metabolism of xenobiotics by cytochrome P450 pathways are closely related to oxidative stress. Further, the content of reactive oxygen species (ROS) in the skeletal muscle tissue of diabetic Chinese hamsters was found to be significantly increased. Oxidative stress is an important factor in T2DM, and 5-oxoprolinase (OPLAH) deficiency has been shown to contribute to heart failure due to oxidative stress [17], motivating us to investigate the role of OPLAH, a downregulated differentially abundant protein, in T2DM. Therefore, we used siRNA to silence OPLAH in human skeletal muscle cells (HSKMCs) and found that this had an effect on insulin resistance and impaired glucose uptake, thus suggesting that OPLAH might be a therapeutic target for T2DM.

2. Material and methods

2.1. Animals

Chinese hamsters were raised in the barrier environment of the Experimental Animal Center of Shanxi Medical University (SCXK2019-0004) with 12 h/12 h alternating light and dark cycles, a constant temperature of 22 ± 2 °C, a humidity level of 50–70%, and unlimited access to food and water. The experimental protocol adopted for the animals was approved by the Experimental Animal Ethics Committee of Shanxi Medical University (Ethics approval number: SYDL2021002).

2.2. Experimental Chinese hamsters and tissue sample preparation

After establishment of the T2DM Chinese hamster model, inbreeding was continued [13]. The standard of Chinese hamsters used for experimentation was as follows [14]: in both groups (diabetic and control), 12-month-old hamsters, half of whom were male, were used. The fasting blood glucose (FBG) levels in the control and diabetic groups were ≤4.5 mmoL/L and ≥6.0 mmoL/L, respectively. Some of the skeletal muscles (gastrocnemius) of the control group (n = 4) and diabetic group (n = 4) were frozen at −80 °C for proteomic testing or for histopathological analysis. Afterwards, some of the skeletal muscles of the control group and the diabetic group were re-selected and frozen in a −80 °C freezer for proteomic differentially abundant protein verification (n = 3) and ROS content detection (n = 6).

2.3. Histopathological examination

The skeletal muscle tissue was embedded in paraffin and sectioned into 4 μm-thin slices. They were then stained with hematoxylin and eosin (HE) and observed under an optical microscope.

2.4. Protein sample preparation

An appropriate amount of skeletal muscle tissue was weighed and ground into powder in liquid nitrogen. Then, four times the volume of the powder was added to lysis buffer for protein dissolution (8 M urea [Sigma Aldrich, Burlington, MA USA] and 1% protease inhibitor cocktail). The mixture was then sonicated, after which the supernatant was collected to detect the protein concentration according to the instructions of the bicinchoninic acid (BCA) kit (Beyotime Biotechnology, China). After adding dithiothreitol (Sigma Aldrich) to the protein solution, it was reduced at 56 °C for 30 min. Iodoacetamide (Sigma Aldrich) was then added and incubated in the dark at room temperature for 15 min. After digestion with pancreatin at 37 °C overnight, additional pancreatin was added to continue enzymatic hydrolysis for 4 h. The polypeptide was then desalted, freeze-dried, dissolved in 0.5 M triethylbenzyl ammonium chloride (Sigma Aldrich), and labeled using the TMT kit (Sigma Aldrich). TMT labeling will have the effect of co-elution, resulting in the ratio compression effect, making the difference in detection smaller than the real difference; to evaluate the effect of co-elution on the ratio, we added a 4:1 ratio of standard protein (MBP) for quality control, and the actual detection ratio was 2.2:1, which was in line with the ratio compression of TMT-labeled item detection; TMT-10 standard reagent was used to label each sample and then mixed for detection. The markers were different to reduce the interfering effect of duplicate labels on the detection, and MS2 was used to test the labeling efficiency of each sample before the omics detection to ensure that the

labeling efficiency in the sample reached at least 97%. The TMT labeling process should be controlled as much as possible for the project. The effect of co-elution on ratio detection was within a controllable range.

2.5. HPLC fractionation

The peptides were labeled and fractionated by high pH reverse-phase HPLC on an Agilent 300Extend C18 (5 μm particle size, 4.6 mm inner diameter, 250 mm long, phaseA: 98% water and 2% acetonitrile; phase B: 98% acetonitrile and 2% water). The peptides were separated on an 8–32% acetonitrile gradient at pH 9 for 60 min, distinguished into 60 components, and finally combined into nine components and vacuum freeze-dried.

2.6. LC-MS/MS analysis

The peptides were dissolved in mobile phase A of liquid chromatography (0.1% (v/v) formic acid aqueous solution (Fluka, USA) and then separated using an EASY-nLC 1000 packed with 1.9 μm/120 Å ReproSil-PurC18 resins (Dr. Maisch GmbH, Ammerbuch, Germany) ultra-high-performance liquid system (mobile phase A: 0.1% formic acid and 2% acetonitrile (Fisher Chemical, Hampton, NH, USA) in water; mobile phase B: 0.1% formic acid and 90% acetonitrile in water). Liquid gradient: 0–52 min, 9–25% B; 52–72 min, 25–35% B; 72–76 min, 35–80% B; 76–80 min, 80% B; flow rate of 350 nL/min; Thermo Fisher Scientific, Waltham, MA, USA). After separation, the solution was injected into the NSI ion source for ionization and analyzed by Orbitrap Fusion Lumos mass spectrometry (ion source voltage: 2.0 kV, primary mass spectrum scan range: 350–1550 *m/z*, scanning resolution: 60,000; secondary mass spectrum scan range: fixed, starting point: 100 *m/z*, secondary scanning resolution: 30,000; Thermo Fisher Scientific). A data-dependent scan program was used to collect data. After the first-level scan, the parent ions of the top 10 peptide fragments with the highest signal intensity were selected and sequentially entered into the HCD collision cell for fragmentation with a fragmentation energy of 32%. Second-level mass spectrometry analysis was also performed sequentially. To utilize mass spectrometry more effectively, the automatic gain control was set to 5E4, the signal threshold was set to 50,000 ions/s, the maximum injection time was set to 70 ms, and the dynamic exclusion time of the tandem mass spectrometry scanner was set to 30 s to avoid repeated scans of precursor ions.

2.7. Database search

MaxQuant (v.1.5.2.8 http://www.maxquant.org/) was used to search for MS mass spectrometry data. The database used was Uniprot_Cricetulus_griseus (23,885 sequences, https://www.uniprot.org, 20,190,315), and a reverse database was added to calculate the false positive rate owing to random matches. Trypsin/P was specified as the cleavage enzyme, which allows for up to four missing cleavages. The mass tolerance for precursor ions was set as 20 ppm in the first search and 5 ppm in the main search, and the mass tolerance for fragment ions was set as 0.02 Da. Carbamidomethyl on Cys was specified as a fixed modification and acetylation modification and oxidation on Met were specified as variable modifications. The quantitative method selected was TMT-10plex, and the false discovery rate for protein identification and PSM identification was set to 1%. A differential expression change or fold-change (FC) of 1.2 was set as the change threshold, and statistical significance was defined as $P < 0.05$. The FC between samples was calculated as the ratio of the TMT reporter ion intensities in the original MS/MS data set. Relative quantification was performed only for peptides specific to a particular protein, and for each sample, quantification was normalized using the average ratio of all unique peptides. Protein quantification was calculated from the median ratio of unique peptides corresponding to a protein when there were at least two unique peptides in a protein.

2.8. Bioinformatics analysis

The UniProt-GOA database (http://www.ebi.ac.uk/GOA/) and the protein sequence algorithm software InterProScan (v.5.14–53.0, http://www.ebi.ac.uk/interpro/) were used to compare the differentially expressed proteins, which were classified according to biological processes (BPs), cellular components (CCs), and molecular functions (MFs). Wolfpsort (v.0.2, http://www.genscript.com/psort/wolf_psort.html) software was used for subcellular location annotation of the differentially expressed proteins. The KEGG automatic automation server (KAAS) (v.2.0, http://www.genome.jp/kaas-bin/kaas_main) was then used to annotate the differentially expressed proteins and pass the KEGG mapper (v2.5, http://www.kegg.jp/kegg/mapper. html), which was matched to the corresponding path in the database. The heatmap.2 function in the R package 'gplots' was used to visualize cluster membership (v.2.0.3, https://cran.r-project.org/web/packages/cluster/). Fisher's exact test was used to identify proteins with abundant differences, and $P < 0.05$ was considered statistically significant.

2.9. Cell culture

HSKMCs were purchased from Huatuo Biotech, cultured in complete medium containing 84% Dulbecco's modified Eagle high glucose medium (Boster, Wuhan, China), 15% fetal bovine serum (CellMax, Beijing China), and 1% penicillin/streptomycin (Solarbio, Beijing, China), and then cultured in a cell incubator at 37 °C with 5% CO_2. When the cell fusion rate reached 70%, the medium was replaced with 2% horse serum (Gibco, Waltham, MA, USA) complete medium to induce differentiation. The medium was changed every other day, and differentiation was completed within approximately 6–7 days. In the group that required additional insulin, the serum-free medium was changed 24 h before adding insulin, after which, 100 nM insulin was added for 30 min.

2.10. Knockdown of OPLAH in HSKMCs

On the third day of cell differentiation, the cells were transfected with siRNA-OPLAH and control siRNA (Hanbio, Shanghai, China; negative control group, NC) using the transfection reagent RNAFit (Hanbio), and the medium was replaced with 2% horse serum medium 12 h after transfection to continue differentiation. Next, mRNA was extracted 48 h after transfection, and protein was extracted 72 h after transfection. The silencing effects of three OPLAH siRNAs were compared. The sequences of siRNAs used to specifically target OPLAH (Hanbio) are shown in Table 1.

2.11. qRT-PCR

TRIzol (Takara, Shiga, Japan) was used to extract total mRNA from the skeletal muscle tissue and cells, and the concentration was determined. The total RNA was then reverse transcribed into cDNA using the PrimeScript™ RT Master Mix kit (Takara, Japan). TB Green®PreMix Ex Taq™II (Takara) was used for quantification using the StepOnePlus Real-Time PCR detection system (Applied Biosystems, Waltham, MA USA), and β-actin was used as an internal reference gene. The relative

Table 1
Sequences of siRNA, specifically OPLAH and control siRNA, used in this study.

Oligo name	Sequences (5′-3′)
OPLAH-siRNA1	Sense: GGCACGUGCGGGUCUUAAATT
	Antisense: UUUAAGACCCGCACGUGCCTT
OPLAH-siRNA2	Sense: GGUGCUGGAGGUGGACGAATT
	Antisense: UUCGUCCACCUCCAGCACCTT
OPLAH-siRNA3	Sense: GAUGUGCAGGUGUUGUUCATT
	Antisense: UGAACAACACCUGCACAUCTT
Control siRNA (NC)	Sense: UUCUCCGAACGUGUCACGUTT
	Antisense: ACGUGACACGUUCGGAGAATT

expression of each gene was calculated using the $2^{-\Delta\Delta Ct}$ method. The primer sequences used (Takara) are listed in Table 2.

2.12. Determination of ROS content

An appropriate amount of skeletal muscle tissue was weighed, immersed in normal saline (μL) with a tissue mass (mg) of seven times, and centrifuged at 3000×*g* for 10 min after ultrasonication. The supernatant was collected to measure the ROS content according to the instructions of the ELISA kit (Jiangsu Meimian Industrial, China). Then, 10 μM of dichloro-dihydro-fluorescein diacetate (DCFH-DA) probe (Nanjing JianCheng, Nanjing, China) was added to each group of cells, and at the same time, 100 μM H_2O_2 was added to the groups that required the addition of H_2O_2, after which the cells were incubated at 37 °C for 1 h and then washed three times with 0.01 M PBS. The cells were observed under a fluorescence microscope. The mean fluorescence intensity values were determined using ImageJ software.

2.13. Determination of glutathione (GSH) content in HSKMCs

After the cells were collected, 0.3 mL of PBS was added to the culture for ultrasonic lysis, and the GSH content was determined according to the instructions provided in the GSH kit (Nanjing Jiancheng).

2.14. 2-[N-(7-nitrobenz-2-oxa-1,3-diaxol-4-yl) amino]-2-deoxyglucose (2-NBDG) uptake in HSKMCs

First, 100 μM of 2-NBDG (Amgicam, Shanghai, China) was added to the cells in each group, and then, the cells were incubated at 37 °C for 1 h, washed with PBS three times, and finally observed under a fluorescence microscope. The mean fluorescence intensity values were analyzed using the ImageJ software.

2.15. Western blotting

After the extraction of skeletal muscle and cellular proteins, they were separated using 10% sodium dodecyl sulfate-polyacrylamide gel electrophoresis, transferred to a nitrocellulose membrane, blocked with 5% skimmed milk powder, and incubated at 4 °C overnight with primary antibodies (SIRT5 [1:1000 dilution; ABclonal, Wuhan, China], ALDH1L1 [1:1000 dilution; ABclonal, Wuhan China], EPHX1 [1:1000 dilution; ABclonal, Wuhan China], GST [1:1000 dilution; ABclonal, Wuhan China], OPLAH [1:1000 dilution; ABclonal, Wuhan, China], p-PI3Kp85α [1:1000 dilution; ABways, Shanghai, China], PI3Kp85α [1:1000 dilution; ABclonal], p-Akt2 [1:1000 dilution; ABclonal], Akt2 [1:1000 dilution; ABclonal], GLUT4 [1:1000 dilution; ABclonal], and β-actin [1:1000 dilution; Bioworld, Beijing, China]). Horseradish peroxidase-labeled goat anti-rabbit or anti-mouse IgG secondary antibodies (1:10000 dilution; Boster, Wuhan, China) were added, after which, the cells were incubated for 1 h at 25 °C. The ECL Plus hypersensitivity reaction luminescence solution (Boster, China) was used for imaging under a chemiluminescence gel system (G: Box Chemi XX9, Syngene UK), and ImageJ software was used to analyze protein bands.

Table 2
List of primers used in this study.

Species	Gene	Primer sequences (5′-3′)	Size (bp)
Cricetulus (Chinese hamster)	SIRT5	F: CGATTCATTCCCCAGTTGTGT	21
		R: CTTGCCATTTTCTCCAATAACCTC	24
	ALDH1L1	F: ATGGAACAGCACCAGGAAGAG	21
		R: AGCCAGCAAAGTAGCGGAAA	20
	EPHX1	F: CTGGAAGACCTGCTGACTAACATC	24
		R: GCACAAAGACCTTCATCCCTTC	22
	GST	F: GGGAGACGGAAGAGGAGAGAA	21
		R: AAGCGATGAAATCCACAAAGCT	22
	OPLAH	F: ACTTTGGAGCAGCCTTTGTTG	21
		R: TCTACGAGGATGGTGCTGTTGT	22
	β-actin	F: AGCCATGTACGTAGCCATCC	20
		R: ACCCTCATAGATGGGCACAG	20
Human	OPLAH	F: GAGCTGCTCTTTCGTGAGG	19
		R: GCGGATCAGCAGGTTTAGG	19
	β-actin	F: CGGGAAATCGTGCGTGACAT	20
		R: AAGGAAGGCTGGAAGAGTGC	20

F = Forward; R = Reverse.

2.16. Statistical rationale

SPSS software (version 23.0; IBM, USA) was used for statistical analysis. Compared with that of genomics and transcriptomics, the quantitative depth of proteomics is relatively low. Relatively few differential proteins can be obtained by quantitative analysis. In the FDR method, to reduce missing too many positive results, a nominal *t*-test *p*-value strategy was used [18]. All values are reported as the mean ± standard error of the mean (mean ± SEM). The Student's t-test was used for comparisons of two groups, and one-way analysis of variance was used for comparisons of more than two groups. Statistical significance was defined as $p < 0.05$.

3. Results

3.1. HE staining of Chinese hamster skeletal muscle

The experimental results of the Chinese hamster FBG and OGTT used in the experiment were published in a previous study [14]. In the control group, the skeletal muscle structure of Chinese hamsters was normal, and the nuclei of the muscle fibers were arranged neatly. In the diabetic group, many muscle fiber nuclei shifted inward and cell spacing increased, indicating that significant pathological changes had occurred in the skeletal muscle tissue (Fig. 1).

3.2. Quantification of skeletal muscle tissue proteins in diabetic hamsters

We obtained 251,895 secondary spectra using mass spectrometry and compared them with those in the database. The number of available effective spectra was 44,202. Among the 15,076 peptides identified, the unique peptide count was 14,358. Of the 2482 proteins identified, 2060 were quantified (Fig. 2A, Table S1). The results of three statistical analysis methods, including principal component analysis, relative standard deviation, and Pearson's correlation coefficients showed good biological repeatability (Fig. S1). In total, 38 differential abundant proteins were identified between the diabetic and control groups ($P < 0.05$, $FC > 1.2$ and $FC < 0.833$), of which 14 were upregulated and 24 were downregulated (Fig. 2B, Table S2). The 38 differentially expressed proteins in the UniProt database and the differential expression between the two groups were clustered using a heat map (Fig. 2C).

3.3. Bioinformatics analysis results

GO functional annotations explained the functions of differentially expressed proteins based on three categories (BP, CC, and MF; Fig. 3A). The BP category was annotated into seven sub-categories, which were mainly involved in metabolic, cellular, and single-organism processes; the CC category was annotated into four sub-categories, mainly in cells and the components of organelles; and the MF category was annotated into eight subcategories, which mainly had catalytic and binding functions. Analysis of the subcellular structure showed that most of the differentially expressed proteins were expressed in the cytoplasm and nucleus, accounting for 31.58% and 21.05% of the 38 proteins, respectively, and 15.79% of the differentially expressed proteins were expressed in both the cytoplasm and nucleus (Fig. 3B).

The functional types of differentially abundant proteins were

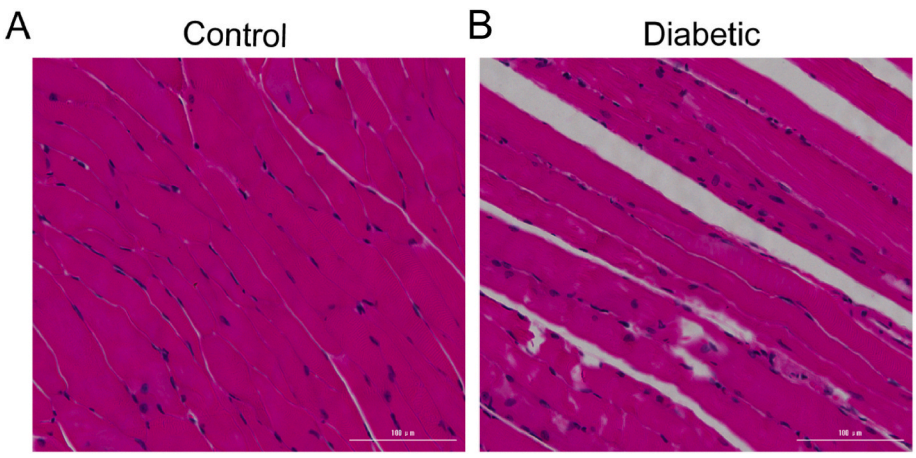

Fig. 1. HE staining of the Chinese hamster skeletal muscle tissue (scale bar, 100 μm). A: Control group (n = 4); B: Diabetic group (n = 4).

determined using GO and KEGG pathway analysis. The bubble chart shows the top 20 GO functional classifications and KEGG pathways that were significantly enriched ($P \leq 0.05$). The BP enrichment results showed that the differentially expressed proteins were mainly related to inorganic ion transmembrane transport (Fig. 3C), whereas the MF enrichment results showed that differentially expressed proteins were mainly related to channel activity and metal ion binding (Fig. 3D). KEGG enrichment analysis showed that the differentially abundant proteins were enriched in six pathways, including ABC transporters, urine metabolism, metabolism of xenobiotics by cytochrome P450, chemical carcinogenesis, glutathione metabolism, and metabolic pathways (Fig. 3E).

3.4. Validation of candidate differentially abundant proteins and determination of ROS content in skeletal muscle tissue

Through KEGG pathway enrichment analysis and a further exploration of the functions of the differentially abundant proteins, five differentially abundant proteins were found to be closely related to oxidative stress. Among them, OPLAH and GST were enriched in the glutathione metabolic pathway and EPHXI and GST were enriched in the metabolism of xenobiotics by cytochrome P450 pathways. These pathways are associated with oxidative stress. Although SIRT5 and ALDH1L1 were not enriched in the pathway, they are also closely related to oxidative stress. Compared with those in the control-group Chinese hamsters, the mRNA and protein levels of SIRT5, ALDH1L1, EPHX1, GST, and OPLAH were decreased in the diabetes group, which was consistent with the proteomic results (Fig. 4A–F). A comparison of these five differentially abundant proteins between the control group and the diabetic group is shown in Table 3. Then, we detected the content of ROS in the skeletal muscle tissue of Chinese hamsters, and the results showed that this was significantly higher in the diabetic group than in the control group (Fig. 4G). Therefore, these five differentially abundant proteins related to oxidative stress might have a certain role. The downregulation of OPLAH has been shown to affect GSH synthesis in myocardial tissue, causing myocardial failure by increasing the level of oxidative stress [17], and oxidative stress can cause IR, which is one of the key factors in the pathogenesis of T2DM [19]. Therefore, we next explored whether the downregulation of OPLAH has an effect on oxidative stress and a role in IR and glucose uptake disorders.

3.5. Knockdown of OPLAH increases oxidative stress levels in HSKMCs

OPLAH plays an important role in the synthesis of GSH, which is an important antioxidant [20]; further, ROS is an important pro-oxidant [21], and thus, after knocking down OPLAH, we determined the level of oxidative stress by detecting the content of GSH and ROS in HSKMCs. First, we silenced OPLAH with siRNA in HSKMCs and detected the knockdown effect by western blotting and PCR. The results showed that OPLAH-siRNA#1 and #2 significantly reduced OPLAH expression, and no effect on the expression of OPLAH was observed in the NC group (Fig. 5A). In the following experiments, we used OPLAH-siRNA#1 and OPLAH-siRNA#2 to knock down OPLAH. Next, we used the kit and DCFH-DA probe to detect the changes in GSH and ROS contents after the knockdown of OPLAH. DCFH-DA is oxidized to 2′-7′ dichlorofluorescein, and the content of ROS can be determined by detecting its fluorescence intensity [22]. The results showed that the knockdown of OPLAH could significantly reduce the intracellular GSH content and increase the intracellular ROS content, especially in H_2O_2 culture conditions (Fig. 5B and C). These results suggest that the downregulation of OPLAH increases the level of intracellular oxidative stress.

3.6. Knockdown of OPLAH plays a role in IR and impaired glucose uptake in HSKMCs

The PI3K/Akt signaling pathway is the main insulin signaling pathway [23]. To determine whether low expression of OPLAH could affect IR, we detected the expression of key proteins in the PI3K/Akt pathway using western blotting. The knockdown of OPLAH reduced the phosphorylation levels of PI3K and Akt, which was not reversed even when this pathway was activated with insulin (Fig. 5D). Skeletal muscle is the largest organ associated with glucose uptake and mainly relies on GLUT4 for glucose transport, which is the main downstream molecule of the PI3K/Akt signaling pathway [24]. Glucose uptake was determined based on the expression of GLUT4 and the fluorescence intensity of 2-NBDG in the cells. 2-NBDG, fluorescently labeled as 2-deoxyglucose, is an optical probe used to detect cellular glucose uptake [25]. The results showed that the knockdown of OPLAH reduced GLUT4 expression and 2-NBDG uptake, regardless of insulin stimulation ($P < 0.05$; Fig. 5D and E). This suggests that the knockdown of OPLAH can inhibit the PI3K/Akt signaling pathway affecting IR, further reducing glucose uptake, and is not affected by insulin.

4. Discussion

Skeletal muscle is composed of many parallel skeletal muscle fibers and surrounding connective tissues, accounting for a collective 40–50% of the total body mass [26]. Symptoms of muscle atrophy and loss of muscle mass are common in patients with T2DM [27,28]. We found that the skeletal muscle tissue of diabetic Chinese hamsters had pathological changes, myocyte nuclei became enlarged and moved inward, and muscle fibers began to atrophy. In the early stage, it was also found that the muscle proportion in diabetic Chinese hamsters was higher than that in the control group [13]. This study aimed to discover the

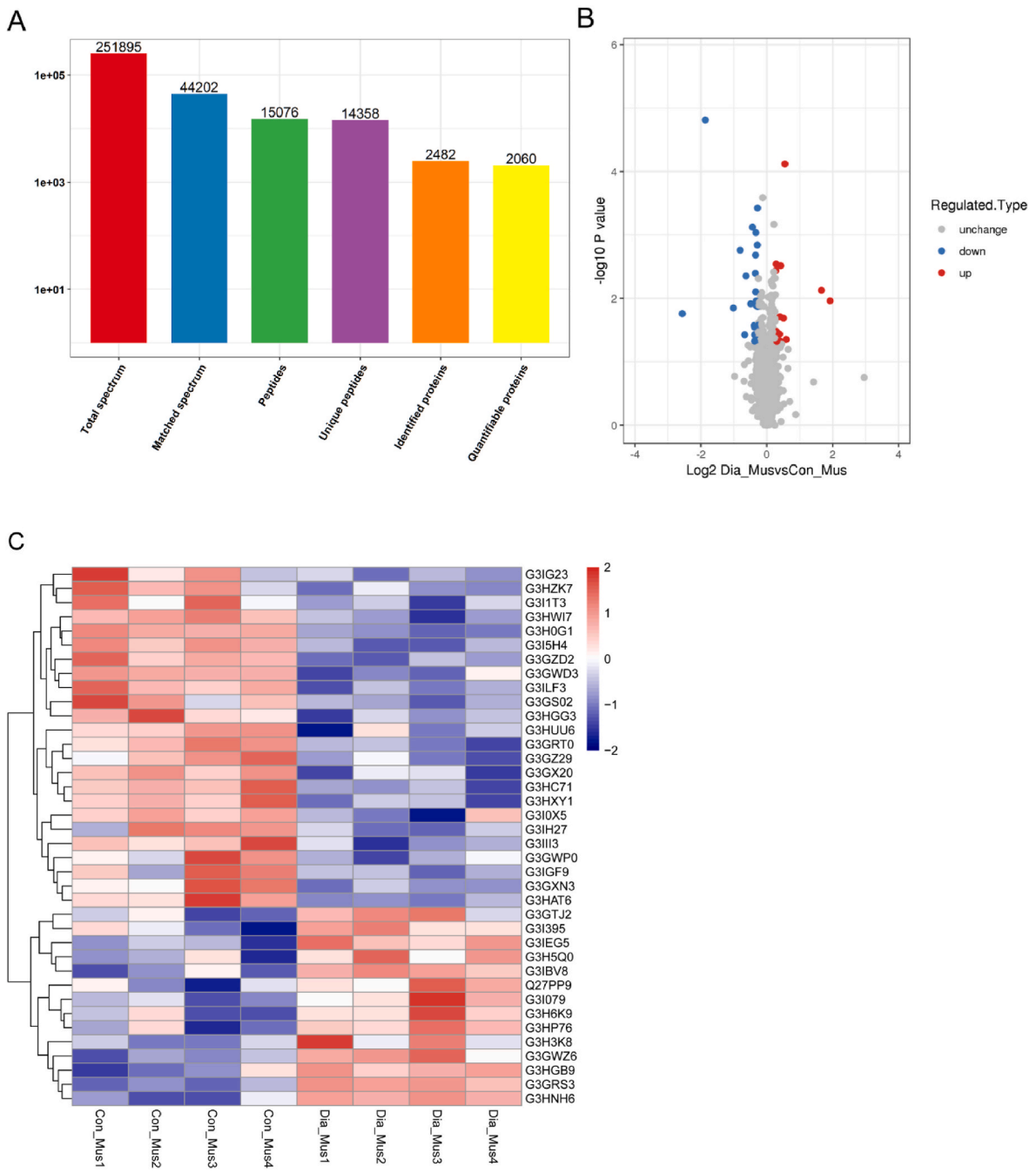

Fig. 2. Quantitative proteomics results and a heatmap of differentially expressed proteins. (A) Results of basic statistical analysis of mass spectrometry data. (B) Differentially expressed protein quantitative volcano plot. The horizontal axis is the value of the relative quantification of protein after Log2 transformation, and the vertical axis is the value after -Log10 transformation of the p-values of the significant difference test. The red and blue dots in the figure represent significantly differentially expressed up- and down-regulated proteins, respectively. (C) Heatmap of differentially expressed proteins. According to the enrichment test (Fisher's exact test) p-value obtained from the enrichment analysis, the hierarchical clustering method is used to cluster related functions in different groups together to form the tree structure of the heatmap.The horizontal axis represents the enrichment results of the tested samples. The vertical axis represents the number of data points in the UniProt database corresponding to the differentially expressed protein. Red and blue blocks represent up- and down-regulated proteins, respectively, and the color intensity represents the degree of difference, with more saturated colors indicating a greater degree of difference. (For interpretation of the references to color in this figure legend, the reader is referred to the Web version of this article.)

characteristics of skeletal muscle tissue lesions in Chinese hamsters through proteomic analysis and provide a new strategy for the study of the pathogenesis of T2DM.

T2DM is a complex disease controlled by multiple genes, and with the extensive application of genome-wide association studies, researchers have discovered more than 300 T2DM susceptibility loci [29]. However, the pathogenesis of T2DM remains unclear. Therefore, continuing to search for potential target genes is still an effective strategy to explore the pathogenesis of T2DM. In this study, a TMT-labeled proteomics analysis was conducted using the skeletal muscle tissue of Chinese hamsters to identify potential targets for T2DM. In the assessment of sample labeling efficiency, we chose MS2 mode, which is more affected by co-elution and the misrecognition rate than MS3 [30]. To reduce this effect, we implemented some alternative

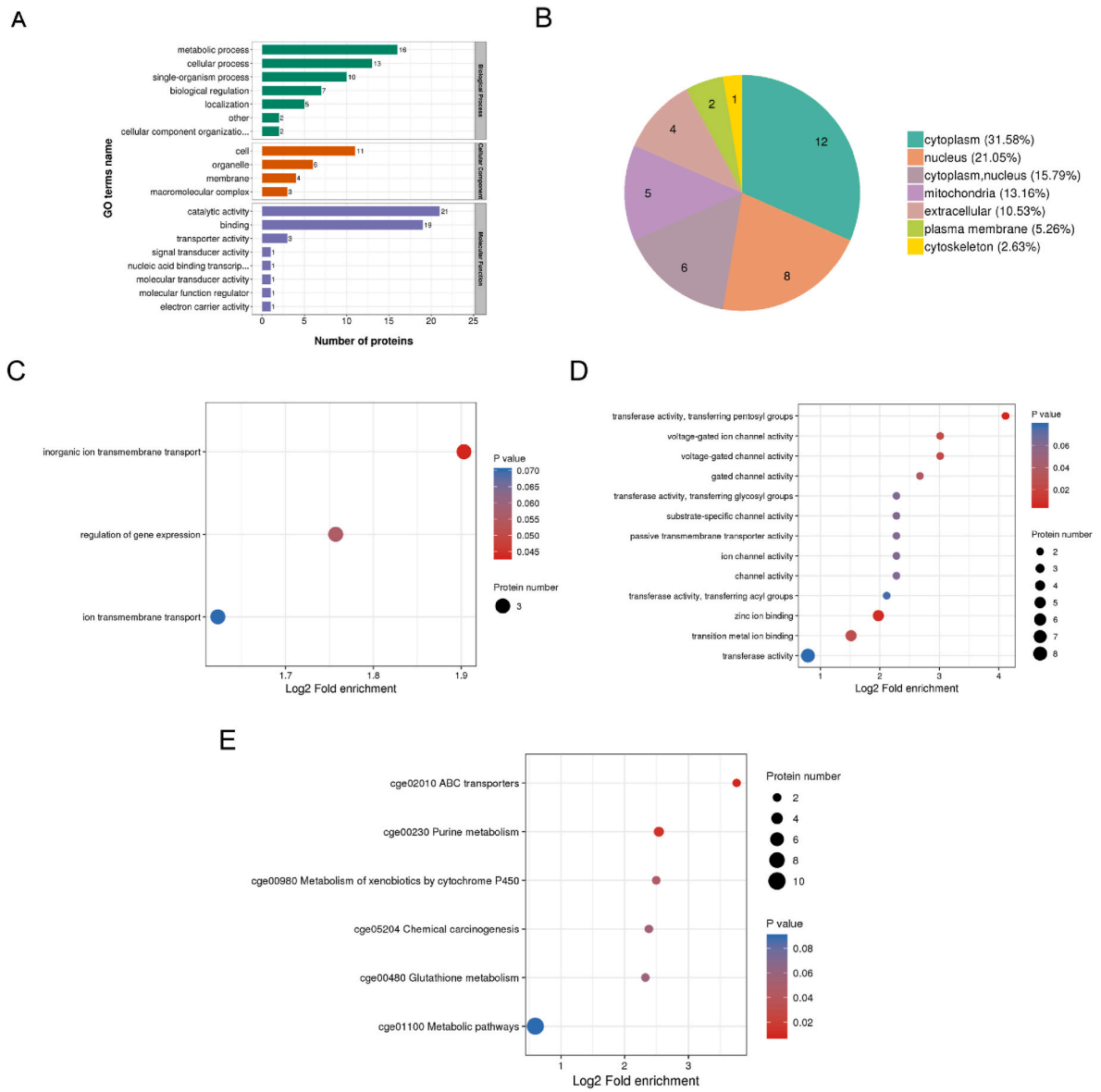

Fig. 3. Gene ontology (GO) secondary functional classification and subcellular structure localization map of differentially expressed proteins (A–B) and bubble plot for functional enrichment analysis of differentially expressed proteins (D-E). (A) Differentially expressed proteins were classified by GO function according to biological processes (BPs), cellular components (CCs), and molecular functions (MFs). (B) Subcellular localization map of differentially expressed proteins. Bubble charts of functional enrichment of differentially expressed proteins in the (C) BP and (D) MF categories. (E) Bubble plot of differentially expressed proteins enriched in the KEGG pathway. The vertical axis in the bubble chart represents the functional classification or pathway, and the horizontal axis represents the Log2-transformed value of the fold change of the proportion of differential proteins in a particular functional type compared to that of the proportion of identified proteins. The color of the circle indicates the significant p-value of enrichment, and the size of the circle indicates the number of differential proteins in the functional class or pathway. (For interpretation of the references to color in this figure legend, the reader is referred to the Web version of this article.)

measures in the experimental scheme, using PIF = 0.75 for filtering during quantification, which can produce a secondary spectrum from the majority of precursor ions in the quantitative results and ensure that the protein is in the identification throughput. At the same time, co-fragmentation is reduced, and we also have graded the sample and divided the sample into 60 components by HPLC, such that the number of peptides in each component is relatively small, which can greatly reduce the impact of co-fragmentation.

Among the six KEGG pathways in which differentially expressed proteins were enriched, glutathione metabolism and metabolism of xenobiotics by cytochrome P450 pathways were all related to oxidative stress. GSH is an antioxidant found in various organelles and is the most common metabolite [20]. Two differentially abundant proteins, OPLAH and glutathione S-transferase (GST), were enriched in the glutathione metabolic pathway. *OPLAH* encodes 5-hydroxyprolinase, which converts 5-hydroxyproline, a degradation product of GSH, into glutamate and participates in the synthesis of GSH [31]. An increase in the 5-hydroxyproline content in the body promotes ROS production and thus oxidative stress [31]. Van der Poel et al. demonstrated that the knockout of OPLAH leads to increased levels of 5-hydroxyproline, affecting GSH synthesis, which in turn leads to increased levels of ROS, resulting in heart failure, and is considered a novel cardioprotective gene [17]. GST is a phase II detoxification enzyme [32]. The detection of GST levels is the basis for the clinical diagnosis of ROS-related diseases [32]. Cytochrome P450 (P450 or CYP) comprises a superfamily of enzymes that oxidize a variety of xenobiotics into chemically reactive metabolites or intermediates, as well as stable metabolites [33]. Two differentially abundant proteins, GST and EPHX1, were enriched in the metabolism of

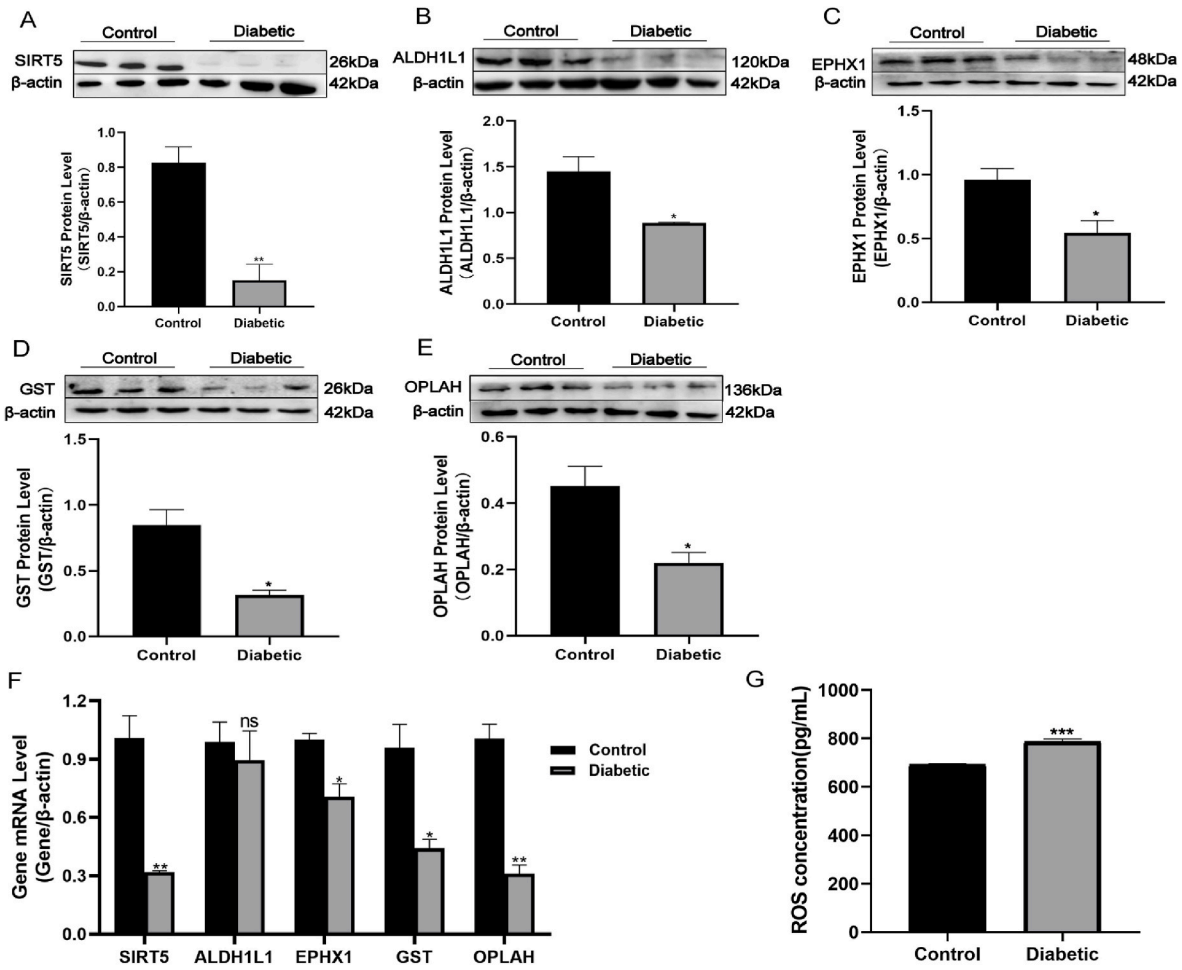

Fig. 4. Validation of candidate differential abundant proteins and determination of reactive oxygen species (ROS) content in Chinese hamsters. (A–E) Candidate differential abundant proteins and β-actin protein levels. (F) Candidate differential abundant proteins and β-actin mRNA levels (n = 3). (G) ROS content (n = 6). All data are presented as mean ± SEM. Statistical significance is denoted as $^{*}p < 0.05$, $^{**}p < 0.01$.

Table 3
Candidate differentially abundant protein information.

NO.	Protein accession[a]	Protein description	Fold change[b]	p-value	KEGG pathway[c]
1	G3H0G1	NAD-dependent protein deacylase sirtuin-5, SIRT5	0.274	0.0000153126	
2	G3GS02	10-formyltetrahydrofolate dehydrogenase, ALDH1L	0.803	0.0130197	cge00670
3	G3I0X5	Epoxide hydrolase 1, EPHX1	0.629	0.037456	cge00980,cge0496, cge05204
4	G3ILF3	Glutathione S-transferase,GST	0.821	0.00144284	cge00480,cge0090, cge00982,cge0110, cge05200,cge0524, cge05225,cge0548
5	G3HWI7	5-oxoprolinase, OPLAH	0.741	0.00075591	cge00480, cge0110

cge00670: One carbon pool by folate; cge00980: Metabolism of xenobiotics by cytochrome P450; cge04976: Bile secretion; cge05204: Chemical carcinogenesis; cge00480: Glutathione metabolism; cge00982: Drug metabolism; cge01100: Metabolic pathways; cge05200: Pathways in cancer; cge05204: Chemical carcinogenesis; cge05225: Hepatocellular carcinoma; cge05418: Fluid shear stress and atherosclerosis.

[a] Number of the protein in the Uniprot database.

[b] The change ratio of protein abundance in diabetic group compared with control group.

[c] Description of the pathway of the protein in the KEGG database.

xenobiotics by cytochrome P450 pathways. EPHX1, also known as mEH, is an epoxide hydrolase that plays a role in xenobiotic metabolism and signal transduction, detoxifies genotoxic compounds, and is involved in the removal of ROS [34,35]. Among the differentially expressed proteins that were not co-enriched in the KEGG pathway, SIRT5 is a regulator of lysine succinylation, malonylation, and glutarylation in mitochondria, which can affect various mitochondrial metabolic pathways. Studies have shown that SIRT5 enhances cellular antioxidant defense by promoting IDH2 desuccinylation and G6PD delipidation [36]. ALDH1L1, also known as 10-formyltetrahydrofolate dehydrogenase (FDH), is responsible for the conversion of 10-formyltetrahydrofolate to tetrahydrofolate and CO_2, and FDH has been shown to enhance cellular antioxidant capacity in zebrafish embryonic cells [37]. The expressions levels of OPLAH, GST, EPHX1, SIRT5, and ALDH1L1 were all down-regulated in diabetic Chinese hamsters, and the ROS content in skeletal muscle tissue of the diabetic group was increased, as shown by ELISA.

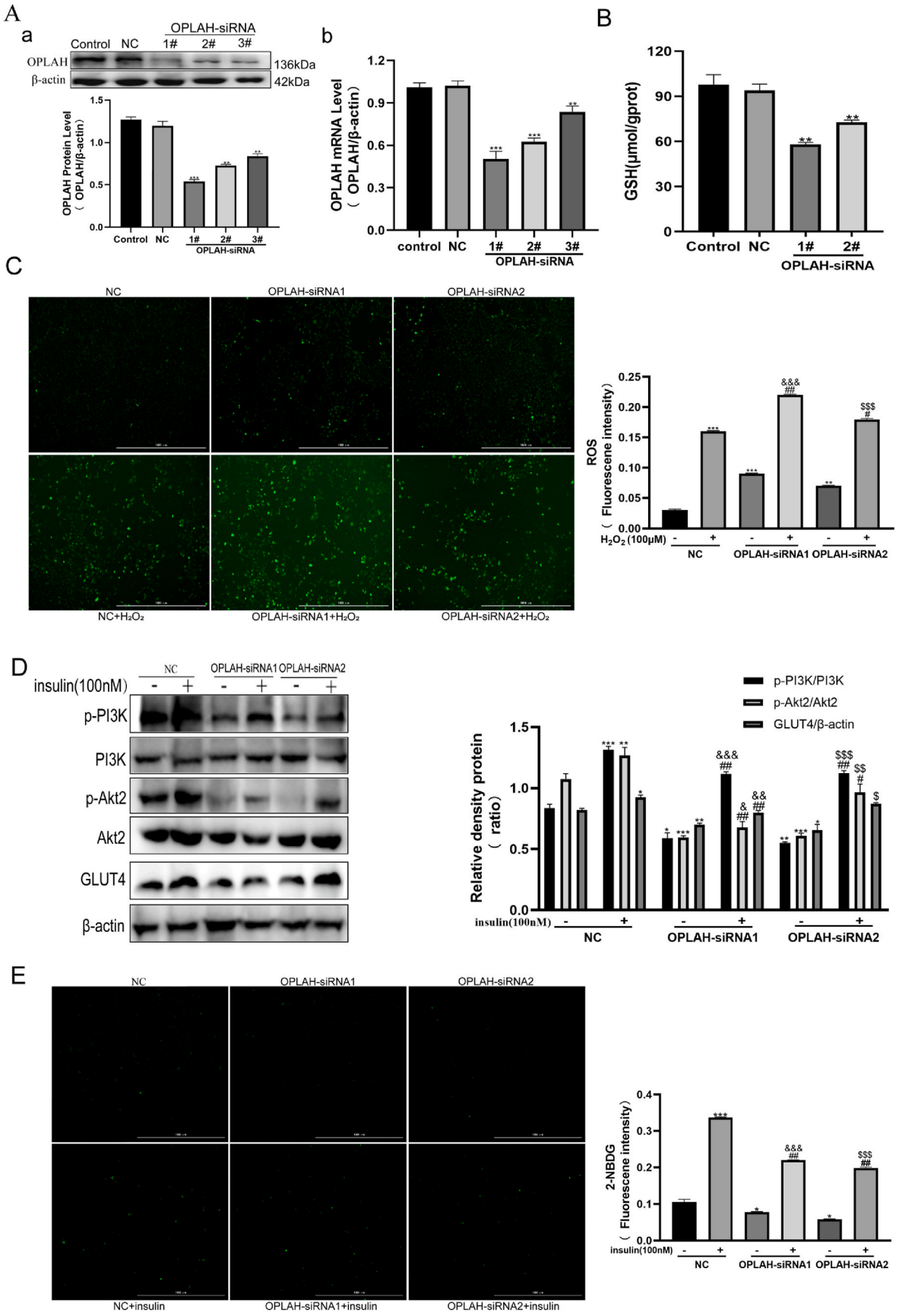

(caption on next page)

Fig. 5. Knockdown of OPLAH causes oxidative stress and inhibits the PI3K/Akt pathway and glucose uptake in HSKMC cells (n = 3). (A) Effects of different specific targeting OPLAH siRNA sequences for silencing. (A-a) Comparison of silencing effects at the protein level. (A-b) Comparison of the silencing effects at the mRNA level. (B–C) Effects of knockdown of OPLAH on GSH and ROS content in HSKMC cells. (B) Effects of knockdown of OPLAH on GSH content. (C) Effects of OPLAH knockdown using a DCFH-DA probe on ROS generation (scale bar: 1000 μm). (D) Knockdown of OPLAH in HSKMC cells inhibited the PI3K/Akt/GLUT4 pathway. After silencing OPLAH, the phosphorylation levels of PI3Kp85α and Akt2 as well as the protein expression of GLUT4 decreased. (E) Knockdown of OPLAH in HSKMC cells inhibited the uptake of 2-NBDG (scale bar: 1000 μm). All data are presented as mean ± SEM. Statistical significance is denoted as: $^{*}p < 0.05$, $^{**}p < 0.01$, $^{***}p < 0.001$ vs. NC; $^{\#}p < 0.05$, $^{\#\#}p < 0.01$, $^{\#\#\#}p < 0.001$ vs. NC + H_2O_2 or NC + insulin; $^{\&}p < 0.05$, $^{\&\&}p < 0.01$, $^{\&\&\&}p < 0.001$ vs. OPLAH siRNA1; $^{\$}p < 0.05$, $^{\$\$}p < 0.01$, $^{\$\$\$}p < 0.001$ vs. OPLAH siRNA2.

Therefore, these five candidate differentially expressed proteins might be related to diabetes in Chinese hamster skeletal muscle tissue associated with increased ROS.

Oxidative stress is one of the important factors that cause many diseases and is related to the pathogenesis of T2DM, IR, and insufficient insulin secretion, which can be a consequence of this [19]. ROS is one of the main enhancers of oxidative stress, and the increase in ROS can lead to a pro-oxidative state in the body, causing damage to the body and IR and affecting glucose uptake by affecting insulin signaling in skeletal muscle cells [38]. Oxidative stress can interfere with insulin signaling by inhibiting the activation of downstream phosphatidylinositol 3-kinase (PI3K) and Akt (protein kinase B), ultimately hindering the transmembrane transport of glucose transporter 4 (GLUT4), which can negatively affect glucose uptake [39]. Therefore, molecules that cause oxidative stress could play a role in IR and glucose uptake and are potential biomarkers for the treatment of T2DM. Among the five differentially expressed proteins identified as having a relationship with oxidative stress, it is known that the knockdown of OPLAH increases the 5-oxyproline content and decreases the GSH content, causes oxidative stress and leading to cardiac damage. In addition, a previous clinical study reported increased 5-hydroxyproline excretion and decreased plasma GSH levels in T2DM patients [40]. Similarly, Murakami et al. also reported lower GSH levels in T2DM patients [41]. Therefore, we further investigated whether OPLAH knockdown had effects on IR and glucose uptake at the cellular level.

PI3K/Akt is an important molecular signaling pathway through which insulin exerts its physiological functions and regulates blood sugar levels, and the decreased activity of any one of the key proteins of this pathway can lead to IR [23]. Whereas both Akt1 and Akt2 are expressed in skeletal muscle, Akt2 was found to be more important for insulin-stimulated glucose uptake [42]. GLUT4 is a major target downstream of Akt and is the main protein for glucose transport in skeletal muscle cells [24]. Akt activation promotes glucose transport by translocating the glucose transporter GLUT4 packaged in GLUT4 storage vesicles to the cell membrane [43]. We silenced OPLAH in HSKMCs and showed that GSH content was reduced, ROS content was increased, the PI3K/Akt pathway was inhibited, and glucose uptake was suppressed. Thus, OPLAH downregulation plays a role in impaired IR and glucose uptake, which might be due to oxidative stress, but the exact mechanism needs to be further identified.

In conclusion, based on TMT proteomics, we screened 38 differentially expressed proteins in the skeletal muscle tissue of a Chinese hamster model and validated five of them that are related to oxidative stress. For the first time, we investigated the relationship between OPLAH and T2DM and found that the downregulation of OPLAH plays a role in IR and impaired glucose uptake. Therefore, we believe that OPLAH might be a promising therapeutic target for the diagnosis and treatment of T2DM.

Author contributions

Zhaoyang Chen, Zhenwen Chen, and Guohua Song designed the study. Zeya Shi performed the experiments and drafted the manuscript. Yitong Huo, Jianan Hou, Ruihu Zhang, Wentao Wang, and Jingjing Yu contributed significantly to sample and data collection. Hailong Wang, Jianqin Wu and Yu Liu guided the experimental work. All authors have approved the final manuscript.

Declaration of competing interest

The authors declare that they have no known competing financial interests or personal relationships that could have appeared to influence the work reported in this paper.

Acknowledgments

This work was supported by the National Natural Science Foundation of China [grant number U21A20194]; and the Shanxi Basic Research Program [grant number 20210302124589]. The authors thank Jingjie PTM BioLab Co. Ltd. (Hangzhou, China) for the mass spectrometry analysis.

Appendix A. Supplementary data

Supplementary data to this article can be found online at https://doi.org/10.1016/j.freeradbiomed.2022.09.029.

References

[1] A.L. Samy, N.N. Hairi, W.Y. Low, Psychosocial stress, sleep deprivation, and its impact on type II diabetes mellitus: policies, guidelines, and initiatives from Malaysia [J], FASEB bioAdvances 3 (8) (2021) 593–600.
[2] H. Sun, P. Saeedi, S. Karuranga, et al., IDF diabetes Atlas: global, regional and country-level diabetes prevalence estimates for 2021 and projections for 2045 [J], Diabetes Res. Clin. Pract. (2021), 109119.
[3] C. Solis-Herrera, C. Triplitt, E. Cersosimo, et al., Pathogenesis of Type 2 Diabetes Mellitus [M], FEINGOLD K R, ANAWALT B, BOYCE A, et al. Endotext. South Dartmouth (MA); MDText.com, Inc. Copyright © 2000-2022, MDText.com, Inc., 2000.
[4] M.C. Petersen, G.I. Shulman, Mechanisms of insulin action and insulin resistance [J], Physiol. Rev. 98 (4) (2018) 2133–2223.
[5] K.E. Merz, D.C. Thurmond, Role of skeletal muscle in insulin resistance and glucose uptake [J], Compr. Physiol. 10 (3) (2020) 785–809.
[6] J.T. Mey, T.P.J. Solomon, J.P. Kirwan, et al., Skeletal muscle Nur77 and NOR1 insulin responsiveness is blunted in obesity and type 2 diabetes but improved after exercise training [J], Physiological reports 7 (6) (2019), e14042.
[7] H.K. Wu, Y. Zhang, C.M. Cao, et al., Glucose-sensitive myokine/cardiokine MG53 regulates systemic insulin response and metabolic homeostasis [J], Circulation 139 (7) (2019) 901–914.
[8] Z.J. Mao, W.S. Xia, F. Chai, Yunpi Heluo decoction attenuates insulin resistance by regulating SIRT1-FoxO1 autophagy pathway in skeletal muscle of Zucker diabetic fatty rats [J], J. Ethnopharmacol. 270 (2021), 113828.
[9] K.A. Sampath, A.G. Maiya, B.A. Shastry, et al., Exercise and insulin resistance in type 2 diabetes mellitus: a systematic review and meta-analysis [J], Annals of physical and rehabilitation medicine 62 (2) (2019) 98–103.
[10] N.B. Robinson, K. Krieger, F.M. Khan, et al., The current state of animal models in research: a review [J], Int. J. Surg. 72 (2019) 9–13.
[11] B. Wang, P.C. Chandrasekera, J.J. Pippin, Leptin- and leptin receptor-deficient rodent models: relevance for human type 2 diabetes [J], Curr. Diabetes Rev. 10 (2) (2014) 131–145.
[12] H. Meier, G. Yerganian, Spontaneous diabetes mellitus in the Chinese hamster (Cricetulus griseus). II. Findings in the offspring of diabetic parents [J], Diabetes 10 (1961) 12–18.
[13] L. Wang, C. Wang, R. Zhang, et al., Phenotypic characterization of a novel type 2 diabetes animal model in a SHANXI MU colony of Chinese hamsters [J], Endocrine 65 (1) (2019) 61–72.
[14] C. Wang, J. Yu, R. Zhang, et al., Small intestine proteomics coupled with serum metabolomics reveal disruption of amino acid metabolism in Chinese hamsters with type 2 diabetes mellitus [J], J. Proteonomics 223 (2020), 103823.
[15] W. Wang, Z. Shi, R. Zhang, et al., Liver proteomics analysis reveals abnormal metabolism of bile acid and arachidonic acid in Chinese hamsters with type 2 diabetes mellitus [J], J. Proteonomics 239 (2021), 104186.
[16] B. Aslam, M. Basit, M.A. Nisar, et al., Proteomics: technologies and their applications [J], J. Chromatogr. Sci. 55 (2) (2017) 182–196.

[17] A. Van der Pol, A. Gil, H.H.W. Silljé, et al., Accumulation of 5-oxoproline in myocardial dysfunction and the protective effects of OPLAH [J], Sci. Transl. Med. 9 (415) (2017).
[18] M. Harel, R. Ortenberg, S.K. Varanasi, et al., Proteomics of melanoma response to immunotherapy reveals mitochondrial dependence [J], Cell 179 (1) (2019) 236–250, e18.
[19] H. Yaribeygi, T. Sathyapalan, S.L. Atkin, et al., Molecular mechanisms linking oxidative stress and diabetes mellitus [J], 2020, Oxid. Med. Cell. Longev. (2020), 8609213.
[20] H.J. Forman, H. Zhang, A. Rinna, Glutathione: overview of its protective roles, measurement, and biosynthesis [J], Mol. Aspect. Med. 30 (1–2) (2009) 1–12.
[21] K. Nowotny, T. Jung, A. HöHN, et al., Advanced glycation end products and oxidative stress in type 2 diabetes mellitus [J], Biomolecules 5 (1) (2015) 194–222.
[22] H. Kim, X. Xue, Detection of total reactive oxygen species in adherent cells by 2',7'-dichlorodihydrofluorescein diacetate staining [J], JoVE : JoVE (2020) 160.
[23] T. Chen, Y. Zhang, Y. Liu, et al., MiR-27a promotes insulin resistance and mediates glucose metabolism by targeting PPAR-γ-mediated PI3K/AKT signaling [J], Aging 11 (18) (2019) 7510–7524.
[24] S. Furuzono, T. Kubota, J. Taura, et al., A xanthene derivative, DS20060511, attenuates glucose intolerance by inducing skeletal muscle-specific GLUT4 translocation in mice [J], Communications biology 4 (1) (2021) 994.
[25] C. Zou, Y. Wang, Z. Shen, 2-NBDG as a fluorescent indicator for direct glucose uptake measurement [J], J. Biochem. Biophys. Methods 64 (3) (2005) 207–215.
[26] S. Schnyder, C. Handschin, Skeletal muscle as an endocrine organ: PGC-1α, myokines and exercise [J], Bone 80 (2015) 115–125.
[27] H. Miyake, I. Kanazawa, K.I. Tanaka, et al., Low skeletal muscle mass is associated with the risk of all-cause mortality in patients with type 2 diabetes mellitus [J], Therapeutic advances in endocrinology and metabolism 10 (2019), 2042018819842971.
[28] B.D. Perry, M.K. Caldow, T.C. Brennan-Speranza, et al., Muscle atrophy in patients with Type 2 Diabetes Mellitus: roles of inflammatory pathways, physical activity and exercise [J], Exerc. Immunol. Rev. 22 (2016) 94–109.
[29] A. Buniello, J.A.L. Macarthur, M. Cerezo, et al., The NHGRI-EBI GWAS Catalog of published genome-wide association studies, targeted arrays and summary statistics 2019 [J], Nucleic Acids Res. 47 (D1) (2019). D1005-d12.
[30] A. Singh, MS3-based cross-link search platform [J], Nat. Methods 17 (2) (2020) 129.
[31] A. Van der Pol, A. Gil, J. Tromp, et al., OPLAH ablation leads to accumulation of 5-oxoproline, oxidative stress, fibrosis, and elevated fillings pressures: a murine model for heart failure with a preserved ejection fraction [J], Cardiovasc. Res. 114 (14) (2018) 1871–1882.
[32] M.C. Martos-Maldonado, J.M. Casas-Solvas, A. Vargas-Berenguel, et al., Electrochemical detection of glutathione S-transferase: an important enzyme in the cell protective mechanism against oxidative stress [J], Methods Mol. Biol. 1208 (2015) 123–138.
[33] T. Niwa, N. Murayama, H. Yamazaki, Oxidation of endobiotics mediated by xenobiotic-metabolizing forms of human cytochrome [J], Curr. Drug Metabol. 10 (7) (2009) 700–712.
[34] M. Decker, M. Arand, A. Cronin, Mammalian epoxide hydrolases in xenobiotic metabolism and signalling [J], Arch. Toxicol. 83 (4) (2009) 297–318.
[35] A.W. Cheong, Y.L. Lee, W.M. Liu, et al., Oviductal microsomal epoxide hydrolase (EPHX1) reduces reactive oxygen species (ROS) level and enhances preimplantation mouse embryo development [J], Biol. Reprod. 81 (1) (2009) 126–132.
[36] L. Zhou, F. Wang, R. Sun, et al., SIRT5 promotes IDH2 desuccinylation and G6PD deglutarylation to enhance cellular antioxidant defense [J], EMBO Rep. 17 (6) (2016) 811–822.
[37] W.N. Chang, G.H. Lee, T.T. Kao, et al., Knocking down 10-Formyltetrahydrofolate dehydrogenase increased oxidative stress and impeded zebrafish embryogenesis by obstructing morphogenetic movement [J], Biochim. Biophys. Acta 1840 (7) (2014) 2340–2350.
[38] Y. Quan, S. Hua, W. Li, et al., Resveratrol bidirectionally regulates insulin effects in skeletal muscle through alternation of intracellular redox homeostasis [J], Life Sci. 242 (2020), 117188.
[39] H.B. Dai, H.Y. Wang, F.Z. Wang, et al., Adrenomedullin ameliorates palmitic acid-induced insulin resistance through PI3K/Akt pathway in adipocytes [J], Acta Diabetol. (2022).
[40] T.E. Forrester, V. Badaloo, F.I. Bennett, et al., Excessive excretion of 5-oxoproline and decreased levels of blood glutathione in type II diabetes mellitus [J], Eur. J. Clin. Nutr. 44 (11) (1990) 847–850.
[41] K. Murakami, T. Kondo, Y. Ohtsuka, et al., Impairment of glutathione metabolism in erythrocytes from patients with diabetes mellitus [J], Metab. Clin. Exp. 38 (8) (1989) 753–758.
[42] H. Cho, J. Mu, J.K. Kim, et al., Insulin resistance and a diabetes mellitus-like syndrome in mice lacking the protein kinase Akt2 (PKB beta) [J], Science 292 (5522) (2001) 1728–1731.
[43] D.T. Li, E.N. Habtemichael, O. Julca, et al., GLUT4 storage vesicles: specialized organelles for regulated trafficking [J], Yale J. Biol. Med. 92 (3) (2019) 453–470.

Further reading

[1] Y. Perez-Riverol, J. Bai, C. Bandla, et al., The PRIDE database resources in 2022: a hub for mass spectrometry-based proteomics evidences [J], Nucleic Acids Res. 50 (D1) (2022) D543-d52.